Energy dependence of the $^4He(\pi^+,\pi^-)$ total cross section

J. Gräter, R. Bilger, H. Clement, R. Meier, and G. J. Wagner
Physikalisches Institut, Universität Tübingen, Auf der Morgenstelle 14, D-72076 Tübingen, Germany

E. Friedman
Racah Institute of Physics, The Hebrew University, Jerusalem 91904, Israel

M. Schepkin
ITEP Moscow, 117218 Moscow, Russia

P. A. Amaudruz, L. Felawka, D. Ottewell, and G. R. Smith
TRIUMF, 4004 Wesbrook Mall, Vancouver, British Columbia, Canada V6T 2A3

A. Ambardar, G. J. Hofman,* M. Kermani,† and G. Tagliente
Department of Physics and Astronomy, University of British Columbia, Vancouver, British Columbia, Canada V6T 2A6

F. Bonutti, P. Camerini, N. Grion, and R. Rui
University and INFN Trieste, 34127 Trieste, Italy

P. Hong, E. L. Mathie, and R. Tacik
University of Regina, Regina Saskatchewan, Canada S4S 0A2

J. Clark and M. E. Sevior
School of Physics, University of Melbourne, Parkville, Victoria 3052, Australia

O. Patarakin
RRC Kurchatov Institut, 123182 Moscow, Russia

(The CHAOS Collaboration)
(Received 21 April 1998)

The total cross section of the $^4He(\pi^+,\pi^-)$ reaction was measured for π^+ kinetic energies ranging from 70 to 130 MeV using the CHAOS spectrometer at TRIUMF and a liquid ^4He target. Around $T_\pi = 90$ MeV, total cross sections exceed conventional model predictions by a factor of 3, whereas at $T_\pi = 70$ MeV and for $T_\pi > 130$ MeV the data are consistent with these calculations. An attempt is made to understand this behavior by assuming the production of the hypothetical d' dibaryon. [S0556-2813(98)03609-7]

PACS number(s): 25.80.Gn, 24.30.Gd, 14.20.Pt

I. INTRODUCTION

At energies in the region of the Δ resonance and above, the pionic double charge exchange (DCX) reaction seems to be fairly well understood [1]. However, around $T_\pi = 50$ MeV the forward angle excitation function for DCX to discrete final states consistently shows a resonancelike structure which so far has not been accounted for by conventional reaction mechanisms.

The inability of conventional calculations to quantitatively reproduce this peculiar energy dependence has prompted an attempt to explain this structure in terms of a resonance with baryon number $B=2$ in the πNN subsystem, the so-called d' [2,3]. According to this hypothesis the observed behavior corresponds to the formation of the d' in the course of the DCX process. This mechanism is capable of consistently reproducing most of the existing data. The parameters of the d' as extracted from the analysis of DCX to final states in nuclei are $m \approx 2.06$ GeV, $\Gamma_{\pi NN} \approx 0.5$ MeV, and $I(J^P) = \text{even}(0^-)$. These quantum numbers prevent the coupling of the d' to the NN channel, thus accounting for the extremely small width of this resonance. Recently a narrow signal consistent with the d' hypothesis has also been observed in the invariant mass spectrum $M_{pp\pi^-}$ of the reaction $pp \rightarrow pp\pi^+\pi^-$ at CELSIUS [4]. As no corresponding signal has been found in the $M_{pp\pi^+}$ spectrum of this reaction, an $I=0$ assignment appears likely. While no distinction of isospin $I=0$ and $I=2$ can be made from the analysis of the DCX experiments, QCD-inspired calculations also tend to favor $I=0$ for such a resonance [5]. In addition, an $I=2$ assignment for the d' would be in conflict with previous dibaryon searches [6,7] in the energy region from 2000 up to 2100

*Present address: University of Colorado, Boulder, CO 80309-0446.

†Present address: Sonigistix Corporation, Richmond, B.C., Canada V7A-5E3.

MeV suggesting the isospin of the d' to be $I=0$.

The DCX reaction to discrete final states is restricted to nuclei with $A \geqslant 7$. For lighter nuclei this reaction can proceed solely to nucleon-unbound continuum states. In the case of DCX on ^{3}He and ^{4}He, these final states consist of identical nucleons. Hence at low energies, where relative S waves between the nucleons are favored, this reaction is Pauli blocked. The d' production threshold lies just in this region of Pauli-suppressed DCX cross section. Therefore, if the d' exists, Pauli blocking is avoided and a sudden rise of the cross section by one order of magnitude can be expected around $T_\pi \approx 80$ MeV [8]. At energies above $T_\pi \approx 120$ MeV the predicted d' cross section drops below the cross section expected from conventional DCX and consequently the cross sections at such energies are no longer sensitive to a possible d' production.

While there exist several measurements of the DCX reaction on ^{4}He [9–14] for incoming π^+ kinetic energies above 100 MeV, no data for this reaction were available below 100 MeV. In this work the total DCX cross sections were measured for incoming pion kinetic energies between 70 and 130 MeV along with the momentum spectra of the outgoing negative pions. While at 70 and 130 MeV only small d' contributions are expected, conventional models differ significantly from predictions including the d' mechanism around 90 MeV. There, the d' hypothesis predicts cross sections that exceed conventional calculations by almost one order of magnitude [8]. Also the predicted momentum distributions provide a means of testing the reaction mechanism. With the mass of the hypothetical d' being around 2.06 GeV the maximum kinetic energy of the decay protons is 25 MeV in the center of mass system of the d'. At such low energies an attractive final state interaction (FSI) between the participating nucleons is effective. Due to this FSI the d' hypothesis predicts a structure for the momentum distributions of the outgoing pions which is significantly peaked towards higher momenta compared to conventional predictions.

A brief account of this work has been published previously [15]. In the present paper we first give experimental details (Sec. II), and then describe the methods of data analysis used (Sec. III) to obtain the results (Sec. IV). We then discuss existing model predictions and introduce an on-shell Monte Carlo model (Sec. V) of the conventional DCX mechanism which is assumed to proceed via two sequential single charge exchange processes. In this part we also recall the prediction based on the exotic reaction mechanism which proceeds via d' formation and decay. Finally, by comparing our excitation function and angle-integrated momentum spectra with various predictions (Sec. VI) we arrive at the conclusions (Sec. VII) concerning the possible contribution of the hypothetical d' resonance to our measured cross sections.

II. EXPERIMENT

A. Apparatus

The apparatus consisted of the CHAOS (Canadian High Acceptance Orbit Spectrometer) detector [16] at the M11 channel at TRIUMF, and a liquid ^{4}He target developed at the University of Regina [17]. CHAOS is a magnetic spectrometer for pion induced reactions whose design was driven by the physical constraints imposed by small cross sections and large backgrounds. CHAOS combines a large angular acceptance with a sophisticated multilevel hardware trigger and the capability of operating at incident pion beam rates of up to 5 MHz. It is based on a dipole magnet that produces a vertical magnetic field of up to 1.6 T. Four concentric cylindrical wire chambers (WC1 to WC4) are placed in the region of the magnetic field which provides a momentum determination of the outgoing particles. The chambers are surrounded by an array of plastic scintillators (ΔE_1, ΔE_2) and lead glass Cerenkov counters (C) for particle identification. The $\Delta E_{1,2}$ and C detectors form the CHAOS fast trigger blocks (CFT) which provide the first level trigger (1LT) by means of the fast scintillator signals. The second level trigger (2LT) uses the wire chamber information to determine, e.g., the polarity of the outgoing tracks. Charged particles are accepted within $\pm 7°$ of the scattering plane (with holes in the regions of the incoming and outgoing beam).

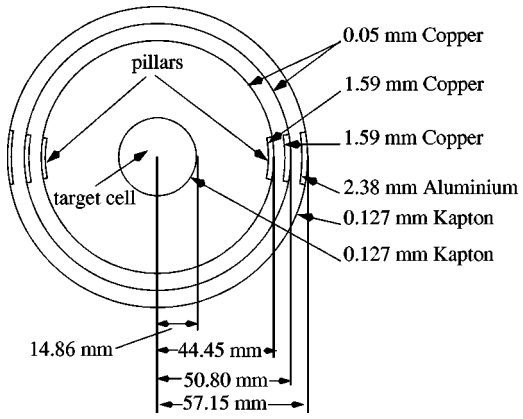

FIG. 1. Schematic top view of the target cell, support pillars, and heat shields.

Since in our experiment most of the outgoing protons were stopped inside the target the expected event multiplicity was one. Nevertheless, the 1LT requirement was set to one or more hits in the CFT blocks to ensure that no good events with an additional proton were lost. While there were no 2LT constraints for elastic scattering, for DCX measurements the 2LT additionally required that the track corresponded to a negatively charged particle.

Incident pions were counted using a plastic scintillator detector (S_0) at the entrance of the spectrometer. The S_0 detector consisted of four 1.6 mm thick and 10 cm high vertical, adjacent strips. The widths of the two inner and outer strips were 8.0 mm and 12.0 mm, respectively.

The liquid ^{4}He target (see Fig. 1) was placed in the center of the detector, inside WC1. It consisted of a cylindrical Kapton cell of 14.9 mm radius, with 127 μm thick walls. This cell was surrounded by two 50 μm thick copper heat-shields at radii of 44.5 and 50.8 mm and a 127 μm Kapton vacuum window at a radius of 57.2 mm. The heat shields and the vacuum window were mounted on two copper pillars of 1.59 mm thickness and an aluminum pillar of 2.38 mm thickness, respectively. The support pillars covered 20° each at opposite sides of the target cell. The target rotation relative to the beam was chosen such that these pillars were placed asymmetrically at 55° and 235° from the beam direction. While the energy loss of pions in the target was typically

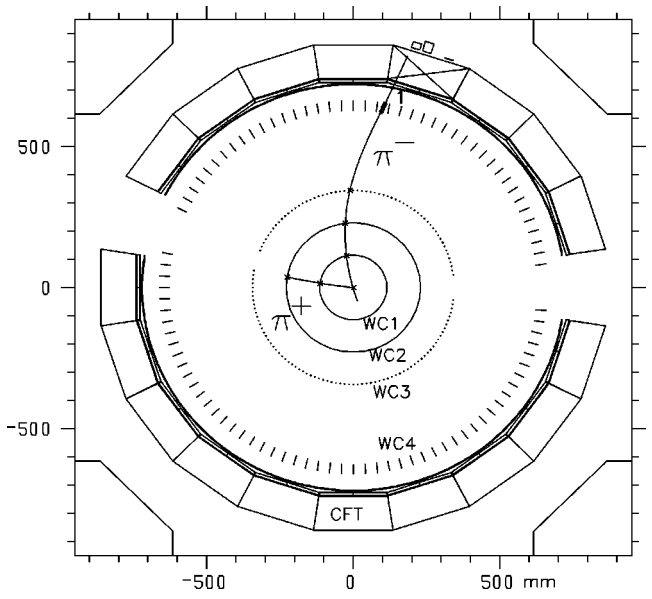

FIG. 2. A DCX event detected in CHAOS. The incoming π^+ interacts in the target volume, the outgoing negative particle leaves a track in the wire chambers and is identified as a π^- in the scintillation and Cerenkov counters. In the region of the incoming and outgoing beam, the drift chambers WC3 and WC4 were switched off because of the high beam rate.

2–4 MeV, protons from the $^4\mathrm{He}(\pi^+,\pi^-)pppp$ reaction were generally stopped in the liquid or the surrounding walls. A typical DCX event where only the outgoing π^- is detected is shown in Fig. 2.

B. Experimental method

The total cross section of the $^4\mathrm{He}(\pi^+,\pi^-)$ reaction was determined by detecting outgoing negative pions within the scattering plane, and extrapolating the finite acceptance to 4π. The data were corrected by means of a Monte Carlo simulation and normalized to π^+-^{4}He elastic scattering. In addition momentum distributions for the outgoing pions were obtained from the measured spectra of the negative pions. Data were taken for the reactions $^4\mathrm{He}(\pi^+,\pi^-)$ (DCX) and $^4\mathrm{He}(\pi^+,\pi^+)$ (el) at channel energies of 70, 80, 90, 100, 115, and 130 MeV. In addition to the runs with liquid ^{4}He in the target, background runs with the empty target were performed at all energies and for both DCX and el trigger settings.

III. DATA REDUCTION

A. Track reconstruction

The wire hit information from the proportional chambers WC1 and WC2 and the drift time information from the drift chambers WC3 and WC4 in conjunction with the CHAOS magnetic field map were used for track and momentum reconstruction using the standard CHAOS track sorting algorithms [16,18]. The principle of the track sorting is that outgoing tracks must be circular, since WC1–WC3 are placed in the region of a homogeneous, vertical field. Therefore, for single track events, the three innermost chambers unambiguously define the outgoing trajectory and its momentum. To reduce ambiguities in multitrack events and improve the momentum resolution of the track reconstruction, the additional information of the vector drift chamber WC4 is taken into account.

B. Particle identification

Particle identification was accomplished by combining the pulse height information from the ΔE_1, ΔE_2, and C counters with the reconstructed particle momenta [19]. For the ΔE_1, ΔE_2 scintillators this results in scatterplots that are similar to those obtained from the well-known ΔE-E technique. While this method provides good discrimination of protons and pions, above 100 MeV pions and electrons are poorly separated. However, in this momentum region the C detectors are a reliable tool for identifying electrons and pions. In a scatterplot of the Cerenkov light versus the particle momentum, electrons form a band that extends to larger pulse heights compared to the pion band. This is because a primary electron creates a shower of secondary electrons which give rise to an enhanced production of Cerenkov light. The main background of negative particles for the DCX measurements resulted from pionic single charge exchange on ^{4}He with subsequent π^0 decay, either directly to final states containing electrons (Dalitz decay) or via conversion of the decay photons. The target pillars located at 55° and 235° were an intense source of such conversion electrons. These electrons appeared in the angular distribution of negative particles as two peaks at scattering angles corresponding to the position of the target pillars. This background reaction was used as a test for the quality of the pion/electron separation by means of the ΔE and C counters. Figure 3 illustrates the efficiency of the particle identification. Figure 3(a) shows the result of a SCX Monte Carlo computer simulation. Indeed, the predicted angular distribution of secondary electrons shows an enhancement at the pillar positions. Figure 3(b) shows the angular distribution of negative particles obtained from experimental DCX data without taking into account the information from the C detectors. Enhancements at scattering angles corresponding to the expected background of electrons from the SCX reaction can be seen. Figure 3(c) is the same as Fig. 3(b) but with the full particle identification, i.e., the C counters were used to separate electrons from pions. At the positions of the background electron peaks of Fig. 3(b) a decrease in the yield is obtained. This is reasonable since not only the electrons are removed from this spectrum but also some pions are lost in the rather massive target pillars. Apart from the above diminutions in regions of the the target pillars and the ones in the regions of the incoming ($\Theta \approx 180°$) and outgoing beam ($\Theta \approx 0°$) the experimental angular distribution is compatible with the assumption of an isotropic distribution of negative pions. Due to beam related background (e.g., beam muons) it was necessary to exclude the CFT block next to the beam exit from the 1LT. Therefore, for the outgoing beam, the uncovered angular region extends to scattering angles up to 30°. We estimate that the systematic error of the integrated total cross sections due to particle identification problems is less than 10%.

C. Total cross sections

The total cross section for the DCX reaction was calculated by integrating doubly differential yields. Those yields

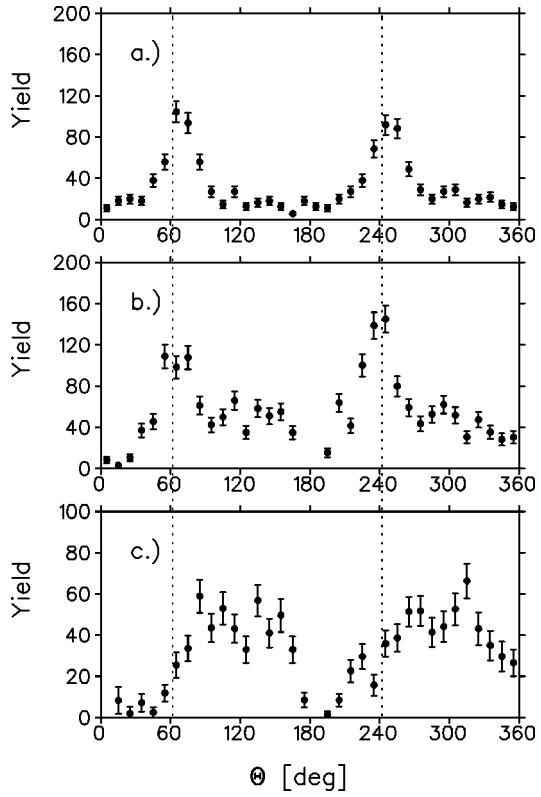

FIG. 3. Angular distributions of outgoing negative particles for an incoming pion energy of 130 MeV. (a) Electron distribution of a computer simulation of the SCX reaction on ^{4}He. (b) Experimental distribution without the pion-electron separation by means of the Cerenkov counters. (c) Same as (b) but with the Cerenkov discrimination of electrons. See text for details.

were obtained by subtracting empty target spectra and applying various correction factors. The normalization was achieved by comparison to elastic scattering data.

The total cross section has the general form

$$\sigma_{\mathrm{DCX}}=\int_{p=0}^{\infty}\int_{\Theta=0}^{\pi}\int_{\Phi=0}^{2\pi}\frac{d^2\sigma_{\mathrm{DCX}}(\Omega,p)}{d\Omega dp}d\Omega dp, \qquad (1)$$

where p is the momentum of the outgoing pion. For the geometry of the CHAOS detector this relation transforms to

$$\sigma_{\mathrm{DCX}}=2\pi f_{\mathrm{mom}}f_{\mathrm{ang}} \times\sum_{p_j=p_{\min}}^{p_{\mathrm{beam}}}\sum_{\Theta_i=0}^{\pi}\frac{d^2\sigma_{\mathrm{DCX}}(\Theta_i,p_j)}{d\Omega dp}\sin\Theta_i\Delta\Theta\Delta p, \qquad (2)$$

where Θ_i is the scattering angle. The quantities f_{mom} and f_{ang} are correction factors that account for the incomplete acceptance of CHAOS in momentum and scattering angle, respectively. The integrations over momentum and solid angle were carried out as summations over angular and momentum bins of $\Delta\Theta=10°$ and $\Delta p=10$ MeV/c, respectively. CHAOS is symmetric in the scattering plane. Therefore, information obtained at scattering angles $\Theta>180°$ was added to the scattering angle $\Theta'=360°-\Theta$.

The doubly differential cross section for DCX in Eq. (2) can be written as

$$\frac{d^2\sigma_{\mathrm{DCX}}}{d\Omega dp}=\frac{Y_{\mathrm{DCX}}(\Theta,p)f_{\mathrm{loss,DCX}}(\Theta,p)}{B_{\mathrm{DCX}}\epsilon_{\mathrm{cham}}\epsilon_{\pi}\epsilon_{\mathrm{tgt}}n_{\mathrm{tgt}}\Delta\Omega\Delta p}. \qquad (3)$$

Similarly, the differential cross section for elastic scattering is given by

$$\frac{d\sigma_{\mathrm{el}}}{d\Omega}=\frac{Y_{\mathrm{el}}(\Theta)f_{\mathrm{loss,el}}(\Theta,p)}{B_{\mathrm{el}}\epsilon_{\mathrm{cham}}\epsilon_{\pi}\epsilon_{\mathrm{tgt}}n_{\mathrm{tgt}}\Delta\Omega} \qquad (4)$$

with the number of events Y, the number of counts B in the beam definition counter S_0, the chamber efficiency ϵ_{cham}, the pion fraction in the beam ϵ_{π}, the fraction of beam hitting the target ϵ_{tgt}, the target density n_{tgt}, and the solid angle $\Delta\Omega$. The factors f_{loss} correct the observed yields for losses due to pion decay, out-of-plane-scattering, energy loss, and the reconstruction efficiency of the analyzing software.

The quantities ϵ_{cham}, ϵ_{π}, ϵ_{tgt}, n_{tgt}, and $\Delta\Omega$ are identical for DCX and elastic scattering. The differential cross section for elastic scattering of positive pions on ^{4}He has been measured previously [20] with high accuracy. With a normalization factor

$$N_{\mathrm{el}}=B_{\mathrm{el}}\frac{d\sigma_{\mathrm{el}}}{d\Omega}\Big/\left(Y_{\mathrm{el}}\,f_{\mathrm{loss,el}}\right), \qquad (5)$$

which was found to be independent of the scattering angle Θ, Eq. (2) can be rewritten as

$$\sigma_{\mathrm{DCX}}=2\pi f_{\mathrm{ang}}f_{\mathrm{mom}}N_{\mathrm{el}} \times\sum_{p_j=p_{\min}}^{p_{\mathrm{beam}}}\sum_{\Theta_i=0}^{\pi}\frac{Y_{\mathrm{DCX}}(\Theta,p)f_{\mathrm{loss,DCX}}(\Theta,p)}{B_{\mathrm{DCX}}}\sin\Theta\Delta\Theta. \qquad (6)$$

The determination of f_{loss}, N_{el}, f_{mom}, and f_{ang} is described below. Table I shows the magnitude of the energy-dependent correction factors for the various pion kinetic energies.

1. Correction factors $f_{\mathrm{loss,DCX}}$ and $f_{\mathrm{loss,el}}$

In order to correct for all pion losses from the target to the CFT blocks computer simulations based on the Monte Carlo program GEANT [21] were used. There were two main reasons for pion losses, namely, losses due to physical processes such as pion decay, energy loss, and multiple scattering and losses due to the reconstruction software. The correction factors were found as the ratios of the number of generated events within the CHAOS acceptance over the number of reconstructed events using a realistic GEANT setup for the CHAOS detector and the standard reconstruction software. Correction factors $f_{\mathrm{loss}}(\Theta,p)$ depending on momentum and scattering angle were obtained for both DCX and elastic scattering. Within the narrow kinematical momentum range of elastically scattered pions the correction factors $f_{\mathrm{loss,el}}$ were constant for a given channel energy. Also, the correction factors $f_{\mathrm{loss,DCX}}(\Theta,p)$ were only slightly dependent on scattering angle and momentum. To give an idea of the magnitude of these correction factors, averaged values $\overline{f_{\mathrm{loss,el}}}$ and $\overline{f_{\mathrm{loss,DCX}}}$ are given in Table I. Note, however, that for the

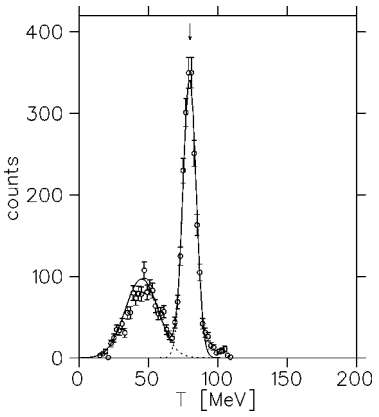

FIG. 4. Energy spectrum of scattered π^+ for the ^{4}He$(\pi^+,\pi^{+\prime})X$ reaction at 90° for an incident pion energy of 100 MeV. The arrow indicates the calculated energy for elastic scattering. The dotted curves represent the Gaussian distributions that were used to extract the elastically scattered pions.

calculation of the total cross section the angular and momentum dependence of $f_{\mathrm{loss,DCX}}(\Theta,p)$ was taken into account.

2. Normalization on elastic scattering N_{el}

Momentum histograms were produced for elastically scattered positive pions (in 10° angular bins) from the runs with 2LT settings for elastic scattering. The elastically scattered pions were clearly separated from the inelastic background due to the large binding energy of ^{4}He. Therefore, the simplest assumption of a Gaussian shape of the inelastic breakup reactions was sufficient to reliably subtract those background reactions (see Fig. 4). The resulting angular-dependent yields $Y_{\mathrm{el}}(\Theta)$ for elastic scattering were multiplied by the averaged factor $\overline{f_{\mathrm{loss,el}}}$ and then fitted to the angular distributions derived from Ref. [20]. In Ref. [20] differential cross sections are given for incoming pion energies of 68, 75, 90, 110, and 130 MeV. Therefore, we had to interpolate the results of Ref. [20] in order to obtain angular distributions at 70, 80, 100, and 115 MeV. The angle-independent normalization factor obtained from this fit is N_{el} of Eq. (5). Figure 5 shows the comparison of the yields from the present experiment and the angular distributions from Ref. [20]. The uncertainty in this fit results in an error of N_{el} of about 5% for all pion kinetic energies.

TABLE I. Energy-dependent correction factors and estimated combined efficiency $\epsilon_{\mathrm{tot}} \equiv \epsilon_{\mathrm{tgt}}\epsilon_{\pi}\epsilon_{\mathrm{chamb}}$, see Sec. III C 2.

T_π [MeV]	f_{mom}	$\overline{f_{\mathrm{loss,DCX}}}$	$\overline{f_{\mathrm{loss,el}}}$	ϵ_{tot}
130	1.12±0.10	1.59±0.08	1.24±0.06	0.46
115	1.17±0.20	1.59±0.08	1.28±0.07	0.41
100	1.24±0.30	1.59±0.07	1.32±0.08	0.33
90	1.41±0.30	1.62±0.07	1.34±0.08	0.25
80	1.71±0.40	1.74±0.08	1.42±0.09	0.25
70	2.0 ±0.80	2.15±0.11	1.46±0.10	0.18

In order to estimate the combined efficiency $\epsilon_{\mathrm{tot}} \equiv \epsilon_{\mathrm{tgt}}\epsilon_{\pi}\epsilon_{\mathrm{chamb}}$ of our experimental setup we used Eq. (4) with values for n_{tgt} and $\Delta\Omega$ derived from geometry. Table I shows the decrease of ϵ_{tot} with energy which was due to the beam characteristics of the M11 channel. At lower energies the pion fraction in the beam diminished rapidly which resulted in a decrease of ϵ_{π} with decreasing energy. In addition, the beam defining slits had to be opened in order to achieve reasonable rates. Therefore, the beam spot on the target was less focused, i.e., ϵ_{tgt} decreased. Note that the efficiency ϵ_{tot} was not used to calculate the total cross section but only served as a rough monitor of the performance of the apparatus.

3. In-plane acceptance correction f_{ang}

The in-plane acceptance correction factor f_{ang} was determined by extrapolating the angle-dependent momentum-integrated quantity $Y_{\mathrm{DCX}}(\Theta)f_{\mathrm{loss,DCX}}(\Theta)$ to in-plane regions that were not covered. Those regions were the beam exit, the beam entrance, and the two regions of the target pillars. Figure 6 shows that outside those regions no dependence on the scattering angle could be observed. Therefore, the extrapola-

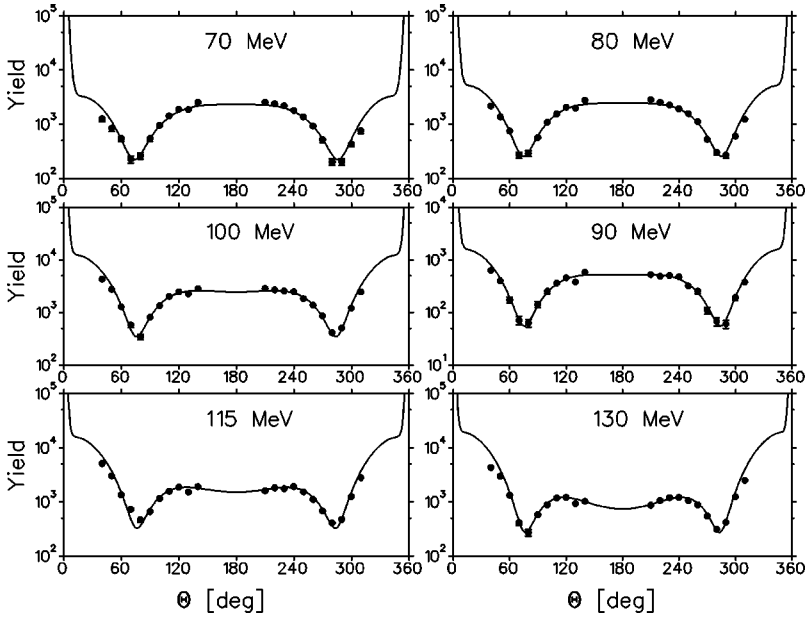

FIG. 5. π^+ ^{4}He elastic scattering yields compared to differential cross sections from Ref. [20].

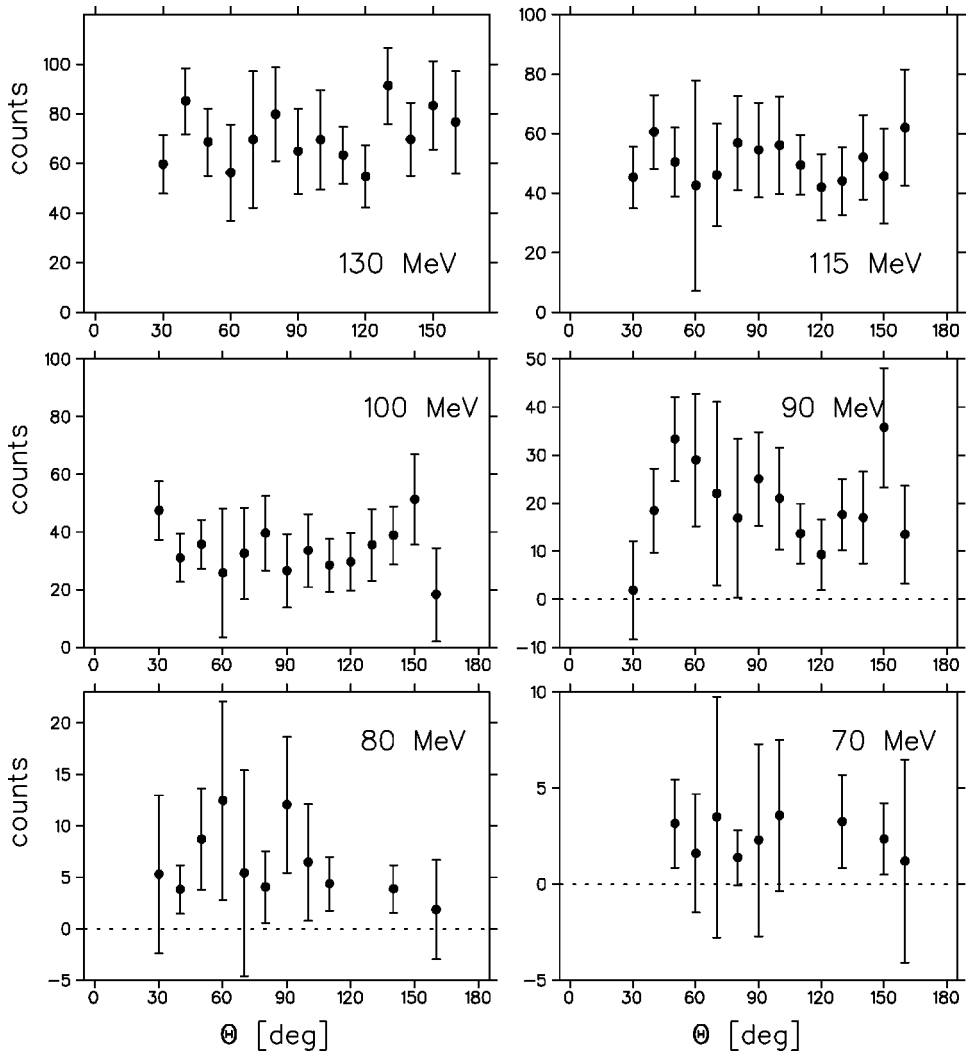

FIG. 6. Angular distributions of the ^{4}He(π^+,π^-) reaction.

tion was performed using a horizontal straight line fit. The regions which were not covered were 0–25°, 165–180° and were the same for all pion kinetic energies. Taking the limited out-of-plane acceptance of CHAOS (±7°) into account, we found $f_{\mathrm{ang}}=10.55$. We estimate an uncertainty of f_{ang} of 5%. Note that since the obtained yields were independent of the scattering angle the assumption of a constant correction factor f_{ang} was justified.

4. Low momentum extrapolation f_{mom}

The momentum threshold for pion detection was about 50 MeV/c, depending somewhat on the incident pion energy and the magnetic field of CHAOS. This threshold was caused by the combined effects of increased energy loss in the target and the strong curvature of low-energy outgoing tracks. The extrapolation of the momentum distributions below the threshold p_{min} was done for the momentum-dependent angle-integrated quantity $Y_{\mathrm{DCX}}(p)f_{\mathrm{loss,DCX}}(p)$. A model-independent spline fit was performed to extrapolate the momentum spectra to zero. The result of this procedure is illustrated in Fig. 7. The extrapolation took into account only the data points that are shown with full dots. The open dots correspond to data points close to the detection threshold p_{min}. The error of this procedure was strongly dependent on the peak position of the momentum spectra and the limited statistics at lower energies. The resulting correction factors f_{mom} and their estimated errors are shown in Table I.

IV. RESULTS

The results for the total cross sections are shown in Fig. 8. Statistical and systematic errors are added quadratically. In Fig. 8 the data from this experiment are also compared to earlier data [9–14]. Note the good agreement of our data with those from other recent measurements [9–12] where the energies overlap. The results are also listed in Table II. In order to focus on the data and not to guide the eye of the reader we have deliberately omitted any theoretical curves for the moment. The angle-integrated momentum distributions above the pion detection threshold are shown in Fig. 7.

V. MODEL CALCULATIONS

There exist various calculations for the DCX reaction on ^{4}He which differ by their level of sophistication as well as by their theoretical approach. In the following we will first give an overview of previous models, then we focus on the Gibbs-Rebka model, and finally introduce a Monte Carlo approach

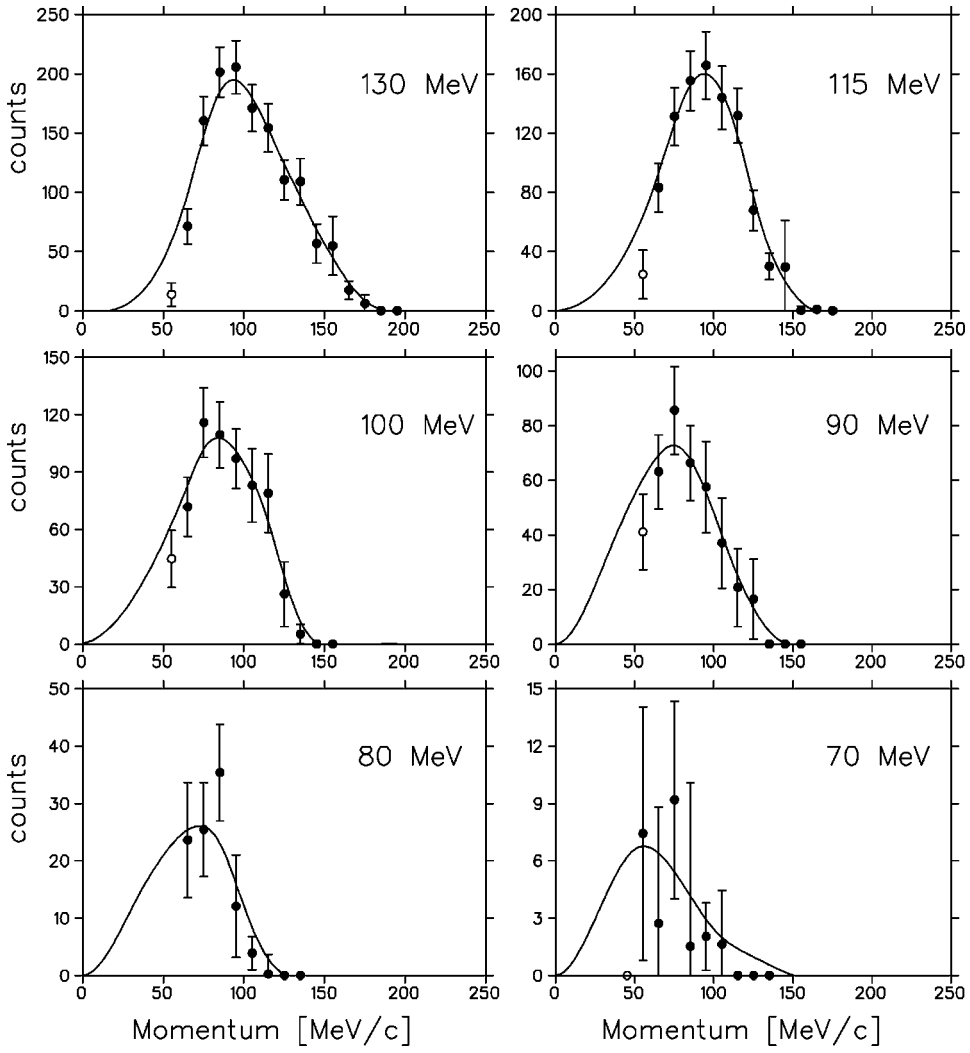

FIG. 7. Momentum distribution of the ^{4}He(π^+,π^-) reaction. The curves are the extrapolations which were used to determine the correction factor $f_{\rm mom}$ due to the low momentum cutoff.

of our own which will allow us to study the influence of various phenomena separately. All these calculations are based on conventional nonexotic mechanisms. In addition, we shall recall the predictions based on the production of the hypothetical d' in Sec. V D.

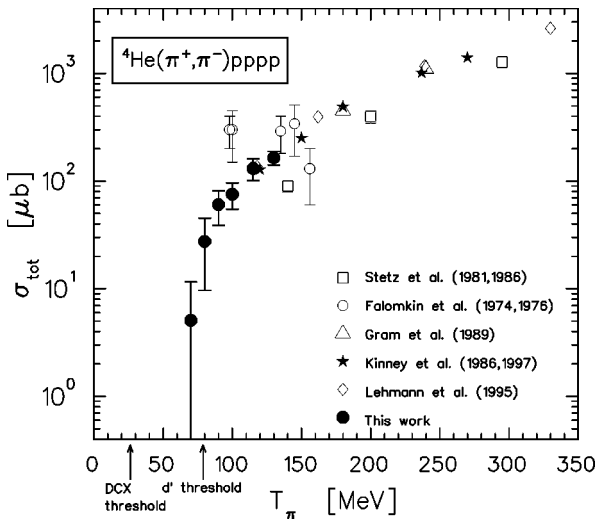

FIG. 8. Experimental ^{4}He(π^+,π^-) total cross sections.

A. Previous models

Becker and Schmit [22] calculated the reaction in a simple impulse approximation assuming the process to proceed via a two-step sequential single charge exchange (SCX) reaction entirely in the P_{33} πN channel. Their predicted cross sections are more than one order of magnitude above the experimental results. The calculations of Jibuti and Kezerashvili [23] as well as those of Germond and Wilkin [24] come much closer to the data for $T_\pi > 130$ MeV. However, at low energies the results of the former calculation are strongly dependent on the NN potential chosen and, therefore, their predictions do not appear reliable enough to test the results of this experiment. The success of the calculation of Germond and Wilkin assuming solely pion scattering on the pion cloud (i.e., exchange currents) must be considered largely fortuitous. It considers the contribution of only one Feynman diagram ($\pi^+ nn \to \pi^- pp$) and completely neglects the two spectator nucleons in the target and hence effects of rescattering, five-particle phase space, and the Pauli prin-

TABLE II. Total cross sections for the reaction ^{4}He(π^+,π^-). The errors are statistical and systematic errors added quadratically.

T_π [MeV]	70	80	90	100	115	130
$\sigma_{\rm DCX}$ [μb]	5 ± 7	27 ± 18	60 ± 21	75 ± 21	131 ± 30	164 ± 24

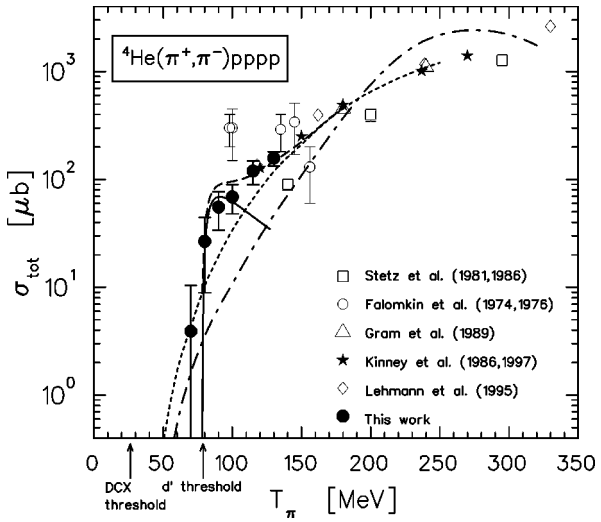

FIG. 9. Total ^{4}He(π^+,π^-) cross sections. The dot-dashed curve shows results from the Gibbs-Rebka model, the dotted curve represents the MC model, the full curve the d' mechanism and the dashed curve the incoherent sum of the MC model and the d' mechanism. See text for details.

ciple. The latter is particularly important at low energies, where the kinematically preferred configuration with four identical nucleons in relative S state must be Pauli blocked. This is demonstrated by the calculations of Gibbs *et al.* [25] which are discussed in the following section. For the sake of completeness we finally mention the calculations of Hüfner and Thies [26] which describe the data with a quality similar to that of Refs. [23–25]. However, they employ a quite different concept based on the Boltzmann equation as an approach to the multiple-scattering problem.

B. Gibbs-Rebka model

The calculation of Gibbs *et al.* assumes the reaction to proceed via sequential SCX similar to Ref. [22]. However, it includes the full πN t matrix, an exact treatment of the five-body phase space and antisymmetrical wave functions. This work has been updated recently by Gibbs and Rebka [27] by implementing more realistic wave functions as well as double Pauli blocking. The effects of Pauli blocking are substantial at low energies. At $T_\pi < 100$ MeV the predicted cross section drops by more than an order of magnitude due to Pauli blocking corrections. For the total DCX cross section the result of this absolute calculation is shown in Fig. 9 by the dot-dashed curve. While this calculation is in qualitative agreement with the experimental results at energies above 120 MeV, it underpredicts our low-energy data by about an order of magnitude. Since a reliable description of the conventional DCX reaction at lower energies is important for the interpretation of our data, we have to consider what shortcomings in the calculation might cause this discrepancy in the energy dependence. Indeed, the only major effect which is not yet incorporated in this calculation and which is thought to play an important role at low energies is the final state interaction (FSI) between the outgoing nucleons. It will counteract the Pauli effects and lead to an enhancement of the cross section at low energies. Since there is no simple and clean way to include the FSI in this fully quantum mechanical calculation, we consider in the following an alternative, semiclassical approach.

C. On-shell Monte Carlo model

In this approach, the DCX reaction ^{4}He(π^+,π^-)$pppp$ is simulated as a two step single charge exchange process. Note that a similar model has been successfully used in previous works [9,11] to describe the measured momentum distributions for $T_\pi > 120$ MeV. Initially, random Fermi momenta are assigned to the four nucleons in ^{4}He. The momenta are distributed according to nucleon momentum distributions extracted from ^{4}He($e,e'p$) data [28]. The incoming π^+ is boosted to the rest frame of one of the neutrons. In this frame, the SCX reaction $n(\pi^+,\pi^0)p$ is carried out, assuming that the energy necessary to break up the ^{4}He nucleus is lost in this first step. The SCX reaction cross section is taken into account by randomly selecting a pion scattering angle and weighting the event according to the laboratory cross section for pion nucleon SCX from SAID [29]. The SAID lab cross sections are taken at an energy 30 MeV above the actual pion energy in order to account for medium effects [9,11].

After the first reaction, the proton and the π^0 are boosted to the laboratory frame and the rest frame of the second neutron, respectively. In the latter the second SCX reaction $n(\pi^0,\pi^-)p$ is performed analogous to the first one. The Pauli principle is introduced by weighting each event with the square of the momenta of the active nucleons as a way of simulating P-wave behavior. A Watson-Migdal-type FSI is taken into account between both the two active nucleons and the two spectator nucleons. To this aim the differential cross sections are weighted with $F_{\rm FSI}$ which was calculated using an eikonal approximation in Ref. [31],

$$F_{\rm FSI}(q) = F_C\left(1 + \frac{(1/R)^2}{F_C^2 q^2 + [(1/2)\rho q^2 - a_s^{-1}]^2}\right) \qquad (7)$$

where the Coulomb correction factor F_C for proton-proton-FSI is given by

$$F_C = \frac{2\pi}{a_c q (e^{2\pi/a_c q} - 1)}. \qquad (8)$$

Here, q is half the relative momentum of the two nucleons, $a_s = -7.8$ fm is the NN scattering length, $\rho = 2.78$ fm is the effective range of the NN potential, and $a_c = 57.5$ fm is the Coulomb scattering length. The parameter R mainly accounts for the interaction range of the FSI. The value of $R = 2.0$ fm used here fits well to calculations and measurements of the FSI in low-energy proton-proton scattering [32]. The result for our calculation with the above parameter is shown as the dashed curve in Fig. 9.

Figure 10 demonstrates the effect of Pauli blocking and FSI on the calculated DCX cross section. Both corrections are quite sizable with almost order-of-magnitude effects on the total cross section—particularly in the steeply rising region above threshold. The Pauli blocking of relative S waves between the four protons indeed shows the expected (see Sec. V B) effect of reducing the rise of the excitation function. The observation that the FSI counteracts this reduction is also plausible. In the limiting case, a strongly attractive

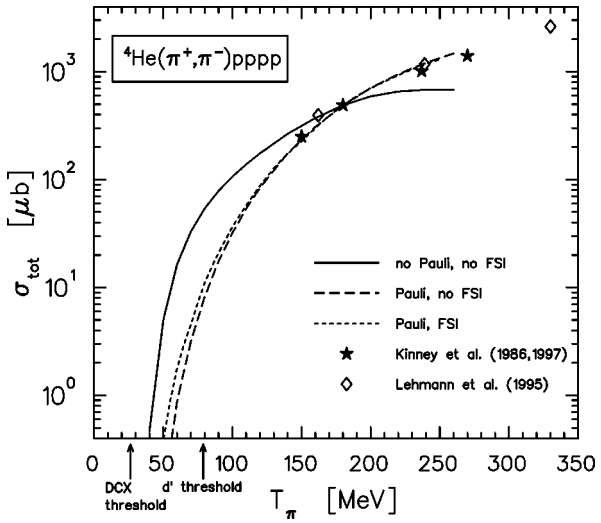

FIG. 10. Results of the Monte Carlo model including various effects such as Pauli blocking and final state interaction (FSI). Also shown are the most recent experimental data above 150 MeV. All curves were normalized at 180 MeV.

FSI produces two diprotons and a pion in the final state and hence a cross section that rises according to a three-body phase space rather than to a five-body phase space.

Our approach provides total cross sections in relative units only and hence the results have to be normalized. We have chosen to normalize at 180 MeV for two reasons. At 180 MeV two recent experiments are fully consistent with each other and no contributions from pion production or d' formation are expected at this energy. The question might arise if this normalization is energy dependent, since competing reaction channels such as pion absorption vary considerably from 70 to 240 MeV. Following the spirit of similar cascade models (e.g., Ref. [30]), at each step of the reaction a SCX process is generated according to its individual strength regardless of the cross section of other possible reaction channels. While direct influence of other channels on the SCX cross section is included implicitly, effects from coupling among the various channels cannot be excluded and are not considered in our approach. However, the results of our calculation describe both the differential and total cross sections of recent data [9,12] for all energies above 150 MeV, if we adjust our normalization constant at one single energy. This success gives confidence that our Monte Carlo (MC) approach provides also a reliable estimate of the conventional DCX cross section at lower energies.

D. The d' prediction

While in conventional models the DCX reaction is assumed to take place predominantly via two sequential SCX processes, the resonant DCX is a one-step process with the d' in the intermediate state. The graphs of these reactions are shown in Fig. 11. Detailed investigations have been undertaken in order to calculate the resonant contribution to the DCX amplitude. The general $\pi NNd'$ vertex was formulated in Ref. [31] and applied to the case of ^{4}He in Ref. [8]. In Ref. [8] FSI effects were incorporated in a similar way as was done in our Monte Carlo approach. This calculation was performed for various ^{4}He wave functions. The prediction of the

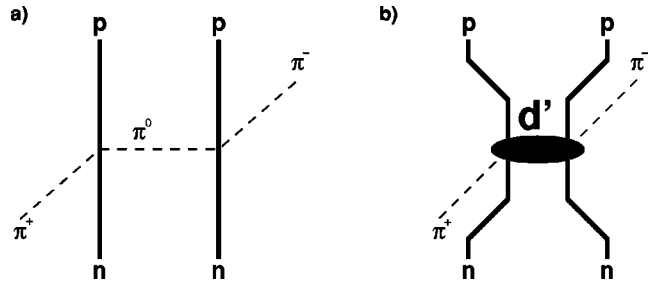

FIG. 11. Graphs of (a) the sequential DCX process and (b) via the intermediate production of the d' resonance.

d' contribution that is based on the wave function of Ref. [8] [see curve (a.) therein] is shown as the full line in Fig. 9.

VI. DISCUSSION

We have presented a variety of conventional calculations of the DCX reaction on ^{4}He. They differ substantially from each other. Among these only our Monte Carlo approach (after normalization) is capable of reproducing the experimental data for energies above 150 MeV. However, a common feature of all these predictions is a smooth behavior of the excitation function at low energies. This is in contrast to the expectation from the formation of the πNN resonance d' in the course of the DCX reaction [8]. This exotic mechanism predicts a steep rise just above the d' production threshold. The dashed curve in Fig. 9 represents the incoherent sum of our Monte Carlo approach and the d' prediction (taken from Ref. [8] without modification). It is seen that our

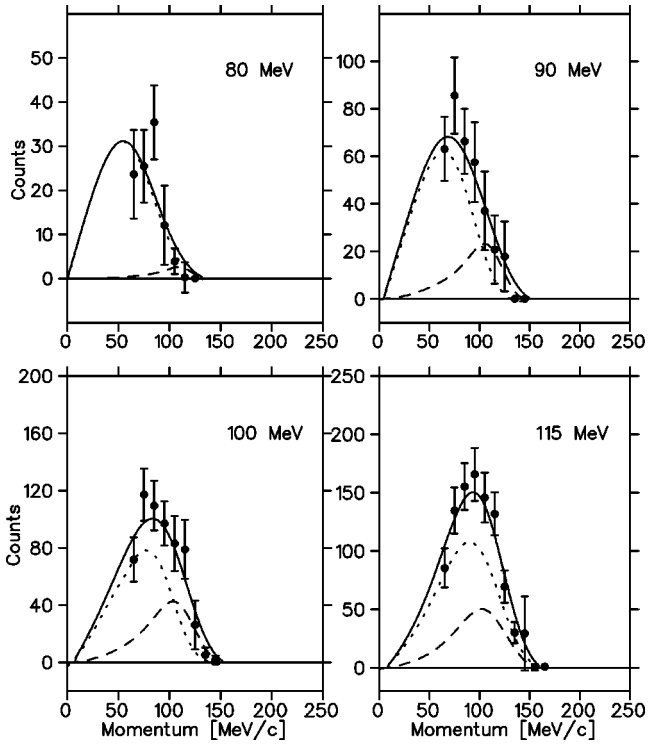

FIG. 12. Momentum distributions for the outgoing π^- at incident pion energies of 80, 90, 100, and 115 MeV. The dotted and dashed curves represent the conventional and the d' mechanism, respectively, with the full curve giving the incoherent sum. See text for details.

low-energy data in addition to the most recent data of Refs. [9, 10] are well described by this sum. Without the inclusion of the d' mechanism the data exceed the Monte Carlo prediction by a factor of 3 around 90 MeV. The quantum-mechanical calculation (Gibbs-Rebka model) underpredicts the data even by an order of magnitude.

The d' hypothesis modifies not only the excitation function but also the momentum distributions of the outgoing pions. As mentioned in the Introduction, in the case of the d' production the momentum spectra are expected to be peaked at somewhat larger momenta compared to the conventional process. In order to test whether the measured momentum spectra require the inclusion of a d' contribution as suggested by the total cross section behavior, we have examined the shape of the momentum distributions. We fitted the incoherent sum of the conventional and of the d' contribution to the experimental data. In this fit procedure the shapes of the respective contributions were kept fixed and only their strengths were adjusted. The result of this procedure is shown in Fig. 12. The best χ^2 was achieved for d' admixtures of $4\pm4\%$, $23\pm12\%$, $32\pm12\%$, and $28\pm18\%$ at 80, 90, 100, and 115 MeV, respectively. The above numbers refer to the d' contribution to the combined (conventional plus d') DCX cross section. Thus at 80 MeV there is no need to include d' contributions which is in contrast to the interpretation of the observed total cross section which suggested a significant d' contribution.

VII. CONCLUSIONS

Using the CHAOS spectrometer at TRIUMF and a liquid ^{4}He target we were able to measure with good accuracy the total cross section of the ^{4}He(π^+,π^-) reaction for six incoming pion kinetic energies between 70 and 130 MeV. In addition momentum spectra of the outgoing π^- were obtained at all energies.

No conventional model is capable of consistently describing the experimental results in the energy range from 70 to 270 MeV. For the total cross section this situation improves considerably with the inclusion of the d' mechanism. Indeed the steep rise predicted to occur at the d' threshold [8] is borne out by the data. Yet, the large differences between the various conventional predictions show that this observation cannot be construed as a proof of the existence of the d'. Such evidence is sought from partially exclusive measurements of the DCX reaction on ^{4}He and ^{3}He. These experiments also used the CHAOS detector at TRIUMF and are trying to obtain πNN invariant mass spectra. The formation of a d' resonance in the intermediate state should give rise to a narrow peak in the respective invariant mass spectrum. Preliminary results of the experiment on ^{4}He have been presented in Ref. [33].

Irrespective of the existence of the d' the total cross sections presented here constitute a considerable extension of the excitation function towards the threshold of the DCX reaction, i.e., into a region that is difficult to access experimentally. It is to be hoped that an increased theoretical effort to understand this few-body reaction will be stimulated by these new low-energy DCX data.

ACKNOWLEDGMENTS

We gratefully acknowledge the assistance provided by the technical and support staff of TRIUMF. This work was supported by the German Federal Minister of Education and Research (BMBF) under Contract No. 06TÜ669 and by the Deutsche Forschungsgemeinschaft (Graduiertenkolleg MU705/3). It received further support from the National Science and Engineering Research Council (NSERC) of Canada and from the Instituto Nazionale di Fisica Nucleare (INFN), Italy.

[1] For a survey see, e.g., N. Auerbach, W. R. Gibbs, J. N. Ginocchio, and W. B. Kaufmann, Phys. Rev. C **38**, 1277 (1988); M. B. Johnson and C. L. Morris, Annu. Rev. Nucl. Part. Sci. **43**, 165 (1993); H. Clement, Prog. Part. Nucl. Phys. **29**, 175 (1992), and references therein.
[2] R. Bilger *et al.*, Z. Phys. A **343**, 491 (1992); R. Bilger, H. Clement, and M. Schepkin, Phys. Rev. Lett. **71**, 42 (1993).
[3] K. Föhl *et al.*, Phys. Rev. Lett. **79**, 3849 (1997).
[4] W. Brodowski *et al.*, Z. Phys. A **355**, 5 (1996).
[5] P. J. Mulders, A. T. Aerts, and J. J. de Swart, Phys. Rev. D **21**, 2653 (1980).
[6] B. Parker *et al.*, Phys. Rev. Lett. **63**, 1570 (1989).
[7] D. Ashery *et al.*, Phys. Lett. B **215**, 41 (1988).
[8] H. Clement, M. Schepkin, G. J. Wagner, and O. Zaboronsky, Phys. Lett. B **337**, 43 (1994).
[9] M. Yuly *et al.*, Phys. Rev. C **55**, 1848 (1997).
[10] A. Lehmann *et al.*, πN Newsletter **11**, 53 (1995).
[11] P. A. M. Gram *et al.*, Nucl. Phys. **A527**, 45c (1991).
[12] E. R. Kinney *et al.*, Phys. Rev. Lett. **57**, 3152 (1986).
[13] A. Stetz *et al.*, Phys. Rev. Lett. **47**, 782 (1981); Nucl. Phys. **A457**, 669 (1986).
[14] L. V. Falomkin *et al.*, Nuovo Cimento A **22**, 333 (1974).
[15] J. Gräter *et al.*, Phys. Lett. B **420**, 37 (1998).
[16] G. R. Smith *et al.*, Nucl. Instrum. Methods Phys. Res. A **362**, 349 (1995).
[17] P. Hong, M.Sc. thesis, University of Regina, 1996.
[18] M. A. Kermani, M.Sc. thesis, University of British Columbia, 1993.
[19] F. Bonutti, S. Buttazzoni, P. Camerini, N. Grion, and R. Rui, Nucl. Instrum. Methods Phys. Res. A **350**, 136 (1994).
[20] B. Brinkmöller and H. G. Schlaile, Phys. Rev. C **48**, 1973 (1993).
[21] GEANT, CERN program library, 1995.
[22] F. Becker and C. Schmit, Nucl. Phys. **B18**, 607 (1970).
[23] R. I. Jibuti and R. Y. A. Kezerashvili, Nucl. Phys. **A437**, 687 (1985).
[24] J. F. Germond and C. Wilkin, Lett. Nuovo Cimento **13**, 605 (1975).
[25] W. R. Gibbs, B. F. Gibson, A. T. Hess, and G. J. Stephenson, Jr., Phys. Rev. C **15**, 1384 (1977).
[26] J. Hüfner and M. Thies, Phys. Rev. C **20**, 273 (1979).

[27] G. Rebka (private communication).
[28] A. Yu. Korchin and A. V. Shebeko, Z. Phys. A **321**, 687 (1985); C. Cioffi, Nucl. Phys. **A463**, 127c (1987).
[29] SAID, SM95 pion nucleon phase shift program (VPI).
[30] L. L. Scaledo, E. Oset, M. J. Vincente-Vacas, and C. Garcia-Recio, Nucl. Phys. **A484**, 557 (1988); **A457**, 669 (1986).
[31] M. Schepkin, O. Zaboronsky, and H. Clement, Z. Phys. A **345**, 407 (1993).
[32] H. Brückmann, W. Kluge, H. Matthäy, L. Schänzler, and K. Wick, Phys. Lett. B **30**, 460 (1969), and references therein.
[33] R. Meier *et al.*, πN Newsletter **13**, 234 (1997).